Low-frequency Raman-scattering study of the liquid-glass transition in aqueous lithium chloride solutions

N. J. Tao, G. Li, X. Chen, W. M. Du, and H. Z. Cummins
Department of Physics, City College of the City University of New York, New York, New York 10031
(Received 7 December 1990; revised manuscript received 28 June 1991)

Raman spectra of 15 and 30 mol % aqueous LiCl solutions were studied in the frequency range 3–350 cm^{-1}, from room temperature to 78 K. At high temperatures, the spectra are very similar to the Raman spectrum of pure water. As the temperature is lowered through the glass transition, the broad central peak that is typical of liquids evolves continuously into a narrow central peak plus a broad band centered near 60 cm^{-1}, both with a depolarization ratio of ~ 0.8. This evolution suggests a common origin for these two features, which are typical of glasses. Comparison of our results with the disorder-induced-scattering model of Martin and Brenig [Phys. Status Solidi B **64**, 163 (1974)], which is often used for glasses, produced poor agreement for both the intensity and depolarization ratio. In an alternative approach, we combined Stephen's [Phys. Rev. **187**, 279 (1969)] second-order Raman-scattering theory for fluids with generalized hydrodynamics and mode-coupling concepts. This approach gave predictions for the depolarization ratio in excellent agreement with our experimental results. It also produced a qualitatively correct description of the low-frequency Raman spectral shape in both the glass and liquid phases.

PACS number(s): 64.70.Pf, 78.30.−j

I. INTRODUCTION

The Raman spectra of amorphous solids (glass) exhibit characteristic low-frequency structure not observed in the spectra of the corresponding crystals. The glass spectra usually exhibit a broad peak (often called the "boson peak") [1] somewhere between ~ 20 and 80 cm^{-1}; below this peak the spectral intensity $I(\omega)$ decreases with decreasing frequency, but again increases at very low frequencies, below ~ 5 cm^{-1}.

These glass Raman spectra have most frequently been analyzed with a disordered-crystal model in which the static frozen-in disorder breaks the usual crystal momentum selection rules, permitting vibrational modes with any wave vector **q** to contribute to the Raman-scattering spectrum. Since this disorder-induced model leads to a low-frequency spectrum $I(\omega) \propto \omega^2$ which vanishes as $\omega \rightarrow 0$, the residual intensity observed at very low frequencies, sometimes designated as the "light-scattering excess," requires an additional mechanism such as the two-state structural-defect-scattering mechanism [2–4], first discussed by Winterling for vitreous silica [5,6].

The disorder-induced-scattering model has been reasonably successful in describing the qualitative shape of the spectrum for some amorphous materials over a limited frequency range [1,7–9]. Its predictions for the scattered intensity and the depolarization ratio, however, have generally shown poor agreement with experimental results [4,7]. (We will return to this point in Sec. III.)

Liquids also exhibit pronounced broadband low-frequency Raman scattering, and it has been observed (in B_2O_3 [10] and $ZnCl_2$ [11], for example) that the spectrum of the liquid evolves continuously into that of the glass as the sample is cooled through the glass transition, again suggesting that the low-frequency Raman spectra of glasses and liquids may have a common origin [12].

The earliest proposed explanation for the low-frequency Raman spectrum of liquids, published in 1928 by Raman and Krishnan [13], attributed the scattering to hindered rotation of anisotropic molecules. This "Rayleigh-wing" mechanism produces a Lorentzian central peak whose width is the inverse of the orientational relaxation time τ_R. Since in typical fluids $\tau_R \sim 10^{-11}$–10^{-12} sec, the width of the Rayleigh wing is ~ 0.5–5 cm^{-1}. In 1968, Levine and Birnbaum [14] showed that binary-collision-induced modification of the molecular polarizability can produce a broad exponential central peak. This intermolecular scattering mechanism fits the experimental data in gases well, but is less successful in fluids where a description limited to binary collisions is usually inadequate [15].

Thibeau, Oskengorn, and Vodar [16] discussed a type of collision-induced scattering in gases due to a specific dipole–induced-dipole (DID) scattering mechanism. In this mechanism the incident optical field induces an oscillating dipole on one molecule, and the field of this dipole polarizes a second molecule which then radiates the scattered light. Stephen [17,18] analyzed the DID mechanism in liquids in a formulation based on hydrodynamic density fluctuations rather than kinetic theory, and applied it to liquid helium to explain the two-roton Raman scattering observed by Greytak and Yan [19]. Stephen's theory was also applied to liquid argon by McTague, Fleury, and DuPre [15], who noted that Stephen's factorization procedure for fourth-order density correlation functions results in an expression for the optical spectrum determined by convolution of the spectra of pairs of density fluctuation modes $S(q,\omega)$ as in second-order Ra-

man scattering, and that the necessary $S(q,\omega)$ data can be obtained from neutron-scattering experiments. Also, Stephen's theory leads to a predicted depolarization ratio ρ of 0.75, independent of frequency and material parameters.

Subsequently, much more work has been done on the collision-induced-scattering problem, much of it by Madden and co-workers [20–24], who have made extensive use of molecular-dynamics calculations to test their models.

Madden and Board [23] and Madden and O'Sullivan [24] noted that the fluctuating polarizability responsible for collision-induced scattering arises from four different mechanisms. The DID term and a second short-range term produce fully depolarized scattering ($\rho=0.75$), while the two other terms, which are important for ionic materials, can produce polarized scattering. Consequently, in simple van der Waals materials, the light scattering is dominated by the DID term and is fully depolarized ($\rho=0.75$). In ionic melts, however, the Coulomb terms are also important and can lead to depolarization ratios substantially less than 0.75, e.g., $\rho\simeq 0.15$ for NaCl [23]. This distinction, depolarization ratios $\rho\sim 0.75$ for simple atomic or molecular fluids but $\rho<0.75$ for ionic melts, is in agreement with a substantial body of observation [25].

Madden [22] has also questioned the validity of the factorization procedure used by Stephen [17,18]. Nevertheless, we will follow Stephen's approach, which allows us to easily connect the Raman spectra with the important density fluctuation modes at wave vectors near the peak of the static structure factor $S(q)$.

Aqueous LiCl solutions have been extensively studied because they are good glass formers in the concentration range of $\sim 11-30$ mol % [26], and also because of their importance in electrochemistry and biochemistry. Furthermore, since the unusual properties of water remain incompletely understood, it is useful to study aqueous solutions in which the solute concentration is an additional experimentally accessible parameter, and in which temperatures much lower than the pure water lower limit of $\sim -30\,^{\circ}\mathrm{C}$ are accessible.

In this paper we report a Raman-scattering study of aqueous LiCl solutions in both the glass and liquid phases. We find that the spectra change continuously with temperature, and also resemble the Raman spectra of pure water. We also find that the depolarization ratio ρ is ~ 0.8 in both the liquid and glass, which agrees with the value for pure water found by De Santis *et al.* [27]. We first compare our results for the glass phase with the disorder-induced-scattering model, and find that the agreement is generally quite poor, particularly for the depolarization ratio. We then present an alternative analysis based on the DID hydrodynamic theory of Stephen [17,18], combined with an expression for the dynamic structure factor $S(q,\omega)$ from the simplified mode-coupling theory of the glass transition. This model provides a unified explanation for the Raman spectra of both the glass and liquid phases, and yields far better agreement with our experimental observations than the disorder-induced-scattering model. The essential new feature of this approach is the critical importance of $S(q_0)$, the structure factor at the wave vector q_0 corresponding to the first coordination shell, which increases rapidly as T is lowered towards the glass transition. In the glass phase, $S(q_0,\omega)$ develops a large static component, which causes the dynamical part of $S(q_0,\omega)$ to become effectively first-order Raman active.

The disorder-induced-scattering model and the molecular-hydrodynamics model employ fundamentally different approaches to describe the light-scattering process. The disorder-induced theory assumes a single first-order scattering event, and results in depolarized scattering only if the transverse acoustic modes are Raman active. In the DID molecular-hydrodynamics theory, the scattering process is second order, and although each dipole is assumed to be fully polarized, the resulting two-step scattering is fully depolarized. This distinction produces the most dramatic difference between the two theories, resulting in predicted depolarization ratios for aqueous LiCl differing by approximately 5.

Our experimental procedures and results are described in Sec. II. In Sec. III we present a brief review of the disorder-induced-scattering model and a comparison of its predictions with our experimental results and with the results of some other experiments. In Sec. IV we develop the hydrodynamic model and also compare its predictions with our results. A summary and conclusions are given in Sec. V.

II. EXPERIMENT

Samples were prepared from Sigma reagent-grade LiCl dissolved in deionized distilled water and filtered through a 0.2-μm membrane filter. The solutions were then transferred to 1-cm-diam glass tubes and flame sealed. The samples were clear with only an occasional dust particle seen to cross the scattering column.

The sample was mounted on the cold finger of an Oxford liquid-nitrogen cryostat, and the temperature was controlled to ± 0.1 K by an Oxford ITC4 temperature controller. 90° Raman spectra, excited by the 4880-Å line of a Coherent model 52 argon-ion laser with typical power at the sample of 100 mW, were obtained with a Spex 1401 tandem grating spectrometer equipped with ISA holographic gratings and conventional photon counting electronics.

Polarized (VV) Stokes Raman spectra of 15 and 30 mol % solutions at temperatures between 294 and 100 K are shown in Fig. 1. At room temperature, the spectra exhibit a broad central mode, a shoulder at ~ 60 cm^{-1}, and a broad band at ~ 180 cm^{-1}. As the temperature is lowered towards the glass transition (~ 140 K for the 15% solution or ~ 165 K for the 30% solution), the central mode narrows and the shoulder near 60 cm^{-1} develops into a distinct band. The gradual change of the broad central mode with its shoulder into a narrow central mode plus a band centered near 60 cm^{-1} suggests that the central mode and the 60-cm^{-1} band have a common origin. We will return to this point later.

The band near 60 cm^{-1} is similar to features observed in the Raman spectra of several other glasses, often designated as the "boson peak," which is usually attributed to

disorder-induced scattering that produces a spectrum mirroring the density of vibrational states [1,7,9,28]. The low-temperature narrow central mode, which evolves continuously from the broad central mode that dominates the spectrum in the liquid phase, corresponds to the "light-scattering excess" observed in other glass systems, which has been attributed to tunneling defect states in the glass [5,7,29]. The 15- and 30-mol % spectra shown in Fig. 1 are very similar, except that the 180-cm^{-1} band in the 15% sample is more intense. We note that there is another weak band at ~ 260 cm^{-1} that becomes more apparent at lower temperatures.

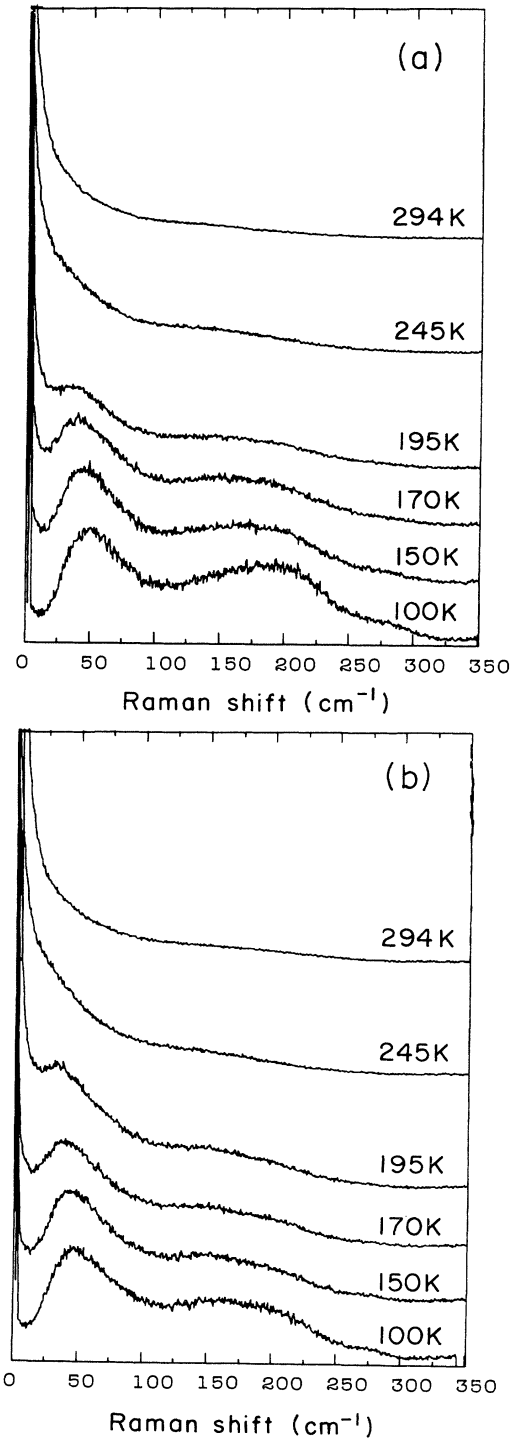

FIG. 1. *VV* polarized Stokes Raman spectra of aqueous LiCl solutions at temperatures between 294 and 100 K. (a) 15 mol % ($T_g \sim 140$ K); (b) 30 mol % ($T_g \sim 165$ K).

We have also measured depolarized (*VH*) spectra of these samples from 294 to 78 K, and found that they are almost identical to (though less intense than) the *VV* spectra. We determined the depolarization ratio $\rho(\omega) = I_{VH}(\omega)/I_{VV}(\omega)$ in the range $3 < \omega < 300$ cm^{-1} at several temperatures, and show the results for the 15% sample in Fig. 2. (The results for the 30% sample were very similar.) The depolarization ratio is ~ 0.8, independent of temperature, from 2 to ~ 130 cm^{-1} and is essentially the same as that of pure water. The fact that the central mode and the band at 60 cm^{-1} have the same depolarization ratio again suggests that they have a common origin. The depolarization ratio at all temperatures exhibits a dip near 180 cm^{-1}, which is visible in Fig. 2. This indicates that the origin of the 180-cm^{-1} band is different from that of the 60-cm^{-1} band and the central mode. Mazzacurati, Nardone, and Signorelli [12] studied the depolarized low-frequency Raman spectrum of 10-M aqueous KOH solution in the liquid and glass phases, and also found that the broad central peak at high temperatures evolves continuously with decreasing temperature, with broad maxima at ~ 60 and 180 cm^{-1} developing at low temperatures. They attributed these maxima to disorder-induced scattering from the TA and LA phonon branches, and identified the temperature dependence of the spectrum with temperature-dependent self-energies of the acoustic phonons. However, they did not investigate either the spectral intensity or the depolarization ratio, which, in analogy with our LiCl results, would probably not be correctly predicted by disorder-induced-scattering models.

The low-frequency Raman spectrum of pure water, which has been reported by several investigators [27,30–34], is very similar to that of aqueous LiCl solutions, including the central mode, the shoulder near 60 cm^{-1}, the band at 180 cm^{-1}, and the weak feature near 260 cm^{-1}, as well as $\rho \simeq 0.75$. Despite extensive study of the Raman spectrum of water, the origin of these features remains controversial. The central component has been decomposed into two Lorentzians [30,35], a narrow Lorentzian attributed to reorientational relaxation of water molecules, and a broad Lorentzian attributed to a hydrogen-bond breaking-reforming process. This decomposition has been challenged recently, however, by Rousset, Duval, and Boukenter [33]. The band at 60 cm^{-1} was assigned to the flexing motion of an O-O-O unit by Walrafen [34,36], while others have assigned it to disorder-induced localized transverse [33,37] or longitudinal [30] acoustic phonons. The band at 180 cm^{-1} was assigned to the O-O stretching mode [34]. We note that in the 30 mol % LiCl solutions, all water molecules belong to LiCl hydration shells, so there is little chance for the formation of O-O-O bridges. If Walrafen's assign-

ment were correct, we should expect a dramatic decrease in the intensity of the 60-cm^{-1} band in the concentrated solutions, which is not observed.

The remarkable similarity between the spectra of aqueous LiCl solutions and water strongly suggests a common origin for the principal features in their spectra. In the water spectra, it has been found that both the 60- and 180-cm^{-1} bands become more pronounced with decreasing temperature, although even at $-27\,^{\circ}$C, the 60-cm^{-1} band was not fully resolved [30]. With our LiCl solutions, we could cool well down into the glass phase, and observed that the 60-cm^{-1} band eventually became fully resolved. Since at low temperatures the 60-cm^{-1} band is very similar to the equivalent feature observed in the Raman spectra of many other glasses, we conclude that the 60-cm^{-1} band in water probably has the same origin as the low-frequency Raman band found in glasses.

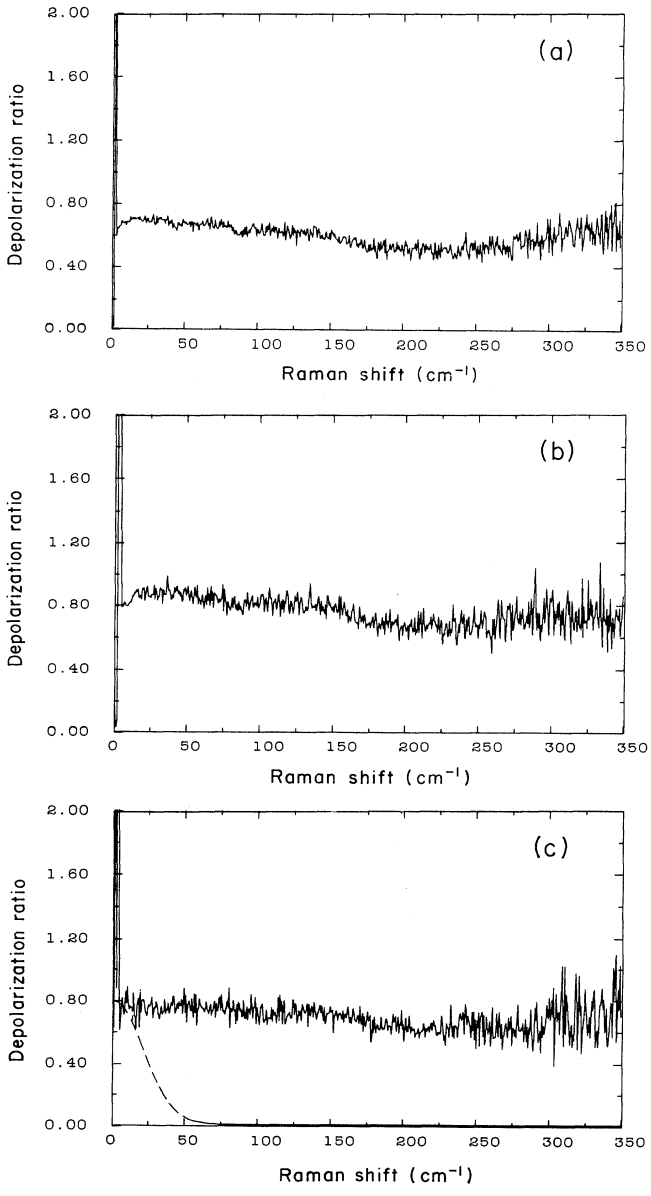

FIG. 2. Depolarization ratio $I_{VH}(\omega)/I_{VV}(\omega)$ of the 15 mol % LiCl solution at T=(a) 294, (b) 245, and (c) 150 K. The dashed line in (c) is the prediction of the Martin-Brenig theory [Eq. (12)], increased by a factor of 5.7.

In order to compare our experimental results with the predictions of the theoretical models to be discussed in Secs. III and IV, we need to know both the spectral intensity $I(\omega)$ at one frequency (which we chose as 20 cm^{-1}) and the integrated low-frequency Raman intensity, both relative to the integrated intensity of the Brillouin line. We first measured the ratio of the Raman intensity to the Rayleigh peak in the Raman spectrum. The Rayleigh peak, meaning the very-low-frequency scattering that was not resolved by the Raman spectrometer, includes the Brillouin peaks, quasielastic scattering due to concentration fluctuations and slow relaxation processes, and (predominantly) elastic scattering from impurities. The same samples were also studied with a tandem interferometer Brillouin spectrometer [38], in which the Brillouin components were fully resolved from the elastic and quasielastic scattering. By combining the results of these two experiments at 200 K, the integrated intensity of the Raman spectrum from 3 to 250 cm^{-1} was found to be $\sim$0.1 of the integrated intensity of the Brillouin components (and was relatively insensitive to temperature), while the Raman spectral intensity at 20 cm^{-1}, integrated over the 1-cm^{-1} bandwidth of the spectrometer, was estimated (relative to the integrated Brillouin component) as 10^{-3}, similar to the value found by Winterling [5] for SiO_2.

III. DISORDER-INDUCED SCATTERING MODEL

Light scattering in condensed matter is produced by inhomogeneous fluctuations $\delta\epsilon(r,t)$ in the dielectric tensor $\epsilon(r,t)=\epsilon_0+\delta\epsilon(r,t)$. For simple scattering geometries (e.g., 90° or 180° VV or VH scattering) the far-field scattered spectral intensity $I_s^{\beta}(\omega_s)$ with polarization β and wave vector $\mathbf{k}_s$ produced by a single scattering event is related to the intensity $I_0^{\alpha}(\omega_0)$ of the incident monochromatic plane-polarized light beam with polarization α, wave vector $\mathbf{k}_0$, and frequency ω_0 by [39]

$$I_s^{\beta}(k_s,\omega_s)=\frac{I_0^{\alpha}V\omega_s^4(n_s/n_I)}{16\pi^2c^4R_0^2}\langle|\delta\epsilon_{\alpha\beta}|^2\rangle_{K\omega}\,, \tag{1}$$

where V is the scattering volume (defined by the optics), R_0 is the distance from V to the detector, $\mathbf{K}=\mathbf{k}_0-\mathbf{k}_s$ is the scattering vector, and $\omega=\omega_0-\omega_S$ is the Raman shift for Stokes scattering. To simplify the equations, we will henceforth use the differential cross section per unit volume $(1/V)(d^2\sigma/d\omega d\Omega)_{\alpha\beta}=I_s^{\beta}(k_s,\omega_s)R_0^2/I_0^{\alpha}V=R_{\alpha\beta}(K,\omega)$.

The quantity $\langle|\delta\epsilon_{\alpha\beta}|^2\rangle_{K\omega}$ in Eq. (1), defined as

$$\langle|\delta\epsilon_{\alpha\beta}|^2\rangle_{K\omega}=\int\int d(t-t')d^3(r-r')e^{iK(r-r')}e^{-i\omega(t-t')}\times\langle\delta\epsilon^*_{\alpha\beta}(r,t)\delta\epsilon_{\alpha\beta}(r',t')\rangle_{r,t}\,, \tag{2}$$

is the K,ω space-time Fourier component of the power spectrum of $\delta\epsilon_{\alpha\beta}$. Note that Eq. (1) applies inside of the sample and must be corrected for reflection and refrac-

tion at the surfaces. Also, for general scattering geometries, $\langle|\delta\epsilon_{\alpha\beta}|^2\rangle$ must be replaced by a sum of quantities $\langle\delta\epsilon^*_{\alpha\beta}\delta\epsilon_{\gamma\delta}\rangle$.

The lattice vibrations of an ideal crystal can be separated into $3N$ branches (j), where N is the number of atoms in the unit cell. For each branch j, the normal mode with wave vector q has the normal coordinate $Q_{qj}(r,t)=Q_{j0}\exp[i(q\cdot r-\omega_{qj}t)]$. The fluctuation $\delta\epsilon_{\alpha\beta}(r,t)$ due to lattice vibrations can be expanded as

$$\delta\epsilon_{\alpha\beta}(r,t)=\sum_{j,q}\left[\frac{\partial\epsilon_{\alpha\beta}}{\partial Q_{jq}}\right]Q_{jq}+\tfrac{1}{2}\sum_{j,q}\sum_{j',q'}\left[\frac{\partial^2\epsilon_{\alpha\beta}}{\partial Q_{jq}\partial Q_{j'q'}}\right]Q_{jq}Q_{j'q'}+\cdots . \quad (3)$$

The first term in Eq. (3) describes one-phonon (first-order) Raman scattering; the second term describes two-phonon (second-order) scattering that produces the weak continuous Raman background in crystals with intensity proportional to the two-phonon joint density of states.

Substituting the first term in Eq. (3) into Eqs. (1) and (2) gives

$$R_{\alpha\beta}(K,\omega)=\frac{\omega_s^4(n_s/n_I)}{16\pi^2c^4}\sum_{j,q}\left|\frac{\partial\epsilon_{\alpha\beta}}{\partial Q_{jq}}\right|^2\langle|Q_{qj}|^2\rangle\times\delta(\mathbf{K}-\mathbf{q})\delta(\omega-\omega_{jq}) . \quad (4)$$

The mode with wave vector $\mathbf{q}=\mathbf{K}$ on each branch contributes a first-order Raman line at $\omega=\omega_{qj}$ with intensity proportional to the square of the polarizability derivative $(\partial\epsilon_{\alpha\beta}/\partial Q_{qj})$, which vanishes unless Q_{qj} and $\epsilon_{\alpha\beta}$ belong to the same irreducible representation of the crystal point group. In deriving Eq. (4), the phonon lifetimes are neglected, which produces the idealized zero-width result $\delta(\omega-\omega_{jq})$. If the (jq) mode has an actual normalized spectrum $s(\omega_{qj})$, then $\delta(\omega-\omega_{qj})$ is replaced by $s(\omega_I-\omega_s)$.

For the acoustic branches in the long-wavelength limit, the normal coordinates are local displacements $u(r,t)$, and the dielectric fluctuations $\delta\epsilon_{\alpha\beta}(r,t)$ are related to the strains $s_{ij}=\frac{1}{2}(du_i/dx_j+du_j/dx_i)$ by $\delta\epsilon_{\alpha\beta}=\epsilon^0_{\alpha\alpha}\epsilon^0_{\beta\beta}\sum_{\gamma,\delta}p_{\alpha\beta\gamma\delta}s_{\gamma\delta}$, where the $p_{\alpha\beta\gamma\delta}$ are Pockel's (photoelastic) coefficients. The thermal average $\langle(qu)^2\rangle=k_BT/2\rho v^2$, where ρ is the mass density, v is the sound velocity, and k_B is Boltzmann's constant. The resulting expressions for the scattering cross section, for 90° VV and VH scattering in an isotropic crystal, are given by [40]

$$R_{zz}(K,\omega)=\left[\frac{\omega_s\epsilon_0}{c}\right]^4\frac{k_BT}{32\pi^2}\frac{p_{12}^2}{\rho v_l^2}\delta(\omega-Kv_l) , \quad (5a)$$

$$R_{zx}(K,\omega)=\left[\frac{\omega_s\epsilon_0}{c}\right]^4\frac{k_BT}{256\pi^2}\frac{(p_{11}-p_{12})^2}{\rho v_t^2}\delta(\omega-Kv_t) , \quad (5b)$$

respectively, where $v_l=(c_{11}/\rho)^{1/2}$ and $v_t=[(c_{11}-c_{12})/2\rho]^{1/2}$ are the longitudinal and transverse sound velocities, respectively. Note that these results are based on a continuum approximation, and are unlikely to apply at wavelengths approaching interatomic distances.

A. Disorder-induced scattering

Since glasses lack the translational symmetry of an ideal crystal, the momentum selection rule implied by $\delta(\mathbf{q}-\mathbf{K})$ in Eq. (4) need not hold. The effects of static disorder on the Raman spectrum were first considered in 1967 by Whalley and Bertie [37]. They discussed a spatially varying Pockels coefficient (which they termed "electrical disorder") $p_{ij}(r)=p^0_{ij}+\delta p_{ij}(r)$, and showed that the $\mathbf{q}$th Fourier component of $\delta p_{ij}(r)$ would cause an acoustic mode at $-\mathbf{q}$ to become Raman active, thereby producing a disorder-induced Raman spectrum proportional to the acoustic density of states. The resulting scattering process thus involves a phonon at $-\mathbf{q}$ and a static fluctuation at $\mathbf{K}+\mathbf{q}$.

In 1970, Shuker and Gammon [28] analyzed the effects of mechanical disorder, which distorts the harmonic vibrational modes from their ideal spatially sinusoidal form. For sufficiently small normal coordinate coherence lengths, they showed that the spectrum $I(\omega)$ is given by

$$I(\omega)\propto\sum_j C_j(1/\omega)[1+n(\omega)]g_j(\omega) , \quad (6)$$

where $g_j(\omega)$ is the density of states of vibrational modes on the jth branch. They also postulated that the coupling constant for the jth branch, C_j, is independent of $\mathbf{q}$.

This assumption of a $\mathbf{q}$-independent coupling constant has led to some confusion, since in the low-frequency limit, where the acoustic modes are dominant and $n(\omega)+1\approx k_BT/\hbar\omega$, Eq. (6) with a $\mathbf{q}$-independent C_j would predict that [11,41] $I(\omega)\propto g_j(\omega)/\omega^2$, so that $I(\omega)$ would be independent of ω. But although the constant coupling approximation is reasonable for optic branches, it is *not* applicable to the acoustic branches. As noted above (and previously pointed out in this context by Winterling [5]), the dielectric modulation $\delta\epsilon(r,t)$ due to acoustic modes is proportional to the strain rather than the displacement, so that the coupling constant C_j for small q acoustic modes must be proportional to q^2. Since $q\propto\omega$ for small q, $C_j\propto\omega^2$, so that Eq. (6) becomes $I(\omega)\propto g_j(\omega)$ rather than $g_j(\omega)/\omega^2$, in agreement with the theoretical analysis of Martin and Brenig described below.

In 1974, Martin and Brenig (MB) [42] combined the ideas of electrical disorder and mechanical disorder in a unified theory of light scattering from acoustic modes in a disordered isotropic continuum. We will illustrate the essential ingredients of their model by considering VV scattering, including only longitudinal-acoustic modes with $\mathbf{q}$ parallel to $\mathbf{K}$. Without disorder, we would have $\delta\epsilon=(\epsilon_0)^2\sum_q p(d/dx)(u_0e^{i(qx-\omega_qt)})$, where $p=p_{12}$ and $\epsilon=\epsilon_{zz}$. Martin and Brenig let $p(r)=p+\delta p(r)$ for electrical disorder, and $u_q(r,t)=u_0e^{iq[x+A(r)]}e^{-i\omega t}$ for mechanical disorder, where $\delta p(r)$ and $A(r)$ are spatially fluctuating quantities produced by the structural disorder. Therefore, the combined $\delta\epsilon$ is

$$\delta\epsilon=(\epsilon_0)^2\sum_q[p+\delta p(r)]\frac{d}{dx}\times\{u_0e^{iqx}[1+i\mathbf{q}\cdot\mathbf{A}(r)+\ldots]\}e^{-i\omega_q t}$$
$$=(\epsilon_0)^2\sum_q[p+\delta p(r)]u_0e^{i(qx-\omega_q t)}\times(iq)\left[1+\frac{d}{dx}\hat{\mathbf{q}}\cdot\mathbf{A}(r)+\ldots\right]. \quad (7)$$

Substituting Eq. (7) in Eq. (2), with the Gaussian ansatz used by MB for the spatial correlation of fluctuations

$$\langle\delta p(r)\delta p(r')\rangle=\langle(\delta p)^2\rangle e^{-(r-r')^2/4\sigma_p^2}$$

and

$$\left\langle p\frac{d}{dx}[\hat{\mathbf{q}}\cdot\mathbf{A}(r)]p\frac{d}{dx'}[\hat{\mathbf{q}}\cdot\mathbf{A}(r')]\right\rangle=\langle(\delta H)^2\rangle e^{-(r-r')^2/4\sigma_A^2},$$

where σ_p and σ_A are the correlation lengths, we have

$$\langle(\delta\epsilon)^2\rangle_{K\omega}=\sum_q\epsilon_0^4q^2\langle u_0^2\rangle\delta(\Omega-\omega_q)\times\int dze^{i(K-q)z}[p^2+\langle(\delta p)^2\rangle e^{-z^2/4\sigma_p^2}+\langle(\delta H)^2\rangle e^{-z^2/4\sigma_A^2}], \quad (8)$$

where $z\equiv r-r'$.

Finally, combining Eqs. (8) and (1), we find

$$R_{VV}(K,\omega)=\frac{1}{16\pi^2}\left[\frac{\omega_s\epsilon_0}{c}\right]^4\sum_q\langle(qu_0)^2\rangle[p^2\delta(\mathbf{K}-\mathbf{q})\delta(\omega-\omega_q)+(4\pi\sigma_p^2)^{3/2}\langle(\delta p)^2\rangle e^{-(K-q)^2\sigma_p^2}\delta(\omega-\omega_q)+(4\pi\sigma_A^2)^{3/2}\langle(\delta H)^2\rangle e^{-(K-q)^2\sigma_A^2}\delta(\omega-\omega_q)]. \quad (9)$$

The first term in Eq. (9), with $\langle(qu_0)^2\rangle=k_BT/2\rho v^2$, recovers the usual first-order Brillouin-scattering result of Eq. (5a). The second and third terms give the electrical- and mechanical-disorder-induced scattering. If the correlation lengths σ_p and σ_A are sufficiently short ($K\sigma\ll1$), then the spectrum of the disorder-induced scattering is proportional to the density of acoustic states: $I(\omega)\sim\omega^4[n(\omega)+1]/\omega$, or, at low frequencies, $I(\omega)\simeq\omega^2$.

The full analysis of the MB model is complicated by the fact that the disorder breaks the momentum selection rule ($\mathbf{q}=\mathbf{K}$) for the direction of $\mathbf{q}$ as well as the magnitude, so that longitudinal- and transverse-acoustic modes propagating in all directions must be included in the integration. The result of the full MB analysis, for 90° *VV* and *VH* disorder-induced scattering, is [4,7]

$$R_{VV}(K,\omega)=\left[\frac{\omega_s\epsilon_0}{c}\right]^4\frac{\omega^2k_BT}{64\pi^2\rho v_l^5}\frac{2}{15}\times\left[(g_t+\tfrac{2}{3}g_l)p_t^2\left[\frac{(\delta p_t^2)}{p_t^2}+\lambda\right]+g_lp_l^2\left[\frac{(\delta p_l^2)}{p_l^2}+\lambda\right]\right], \quad (10a)$$

$$R_{VH}(K,\omega)=\left[\frac{\omega_s\epsilon_0}{c}\right]^4\frac{\omega^2k_BT}{64\pi^2\rho v_l^5}\times\left[\frac{1}{10}(g_t+\tfrac{2}{3}g_l)p_t^2\left[\frac{(\delta p_t^2)}{p_t^2}+\lambda\right]\right], \quad (10b)$$

where $p_l=(p_{11}+2p_{12})/3$, $p_t=(p_{11}-p_{12})$, $\lambda=\langle[(\partial/\partial x_{11})\hat{\mathbf{q}}\cdot\mathbf{A}(r)]^2\rangle$, $g_l(\omega)=\exp[-(2\pi\omega c\sigma/v_l)^2]$, $g_t(\omega)=(v_l/v_t)^5\exp[-(2\pi\omega c\sigma/v_t)^2]$ (where ω is in cm^{-1}), and $\sigma_A=\sigma_p=\sigma$ is the structural correlation length.

Equations (10) provide explicit predictions of the MB theory for the spectral shape, depolarization ratio, and intensity of the low-frequency Raman spectra of glasses in terms of the parameters σ, λ, $\langle(\delta p_l)^2/p_l^2\rangle$, and $\langle(\delta p_t)^2/p_t^2\rangle$.

B. Comparisons with experiment

1. Spectral shape

In the low-frequency limit $\omega\ll v_t/2\pi c\sigma$ (or, equivalently, $q\sigma\ll1$), Eqs. (10) predict that both I_s^{VV} and I_s^{VH} are proportional to ω^2. Experimentally, the prediction $I_{(\omega\to0)}\to0$ is not observed, since there is usually a "light-scattering excess" below $\sim5\ \mathrm{cm}^{-1}$. At higher frequencies, Eqs. (10) predict that, because of the finite correlation length σ, $I(\omega)$ falls below ω^2 as ω approaches $v_t/2\pi c\sigma$. The parabolic spectral shape $I(\omega)\propto\omega^2$ has been shown to fit the experimental spectra of some materials in a limited frequency range, e.g., from ~5 to $\sim20\ \mathrm{cm}^{-1}$ in As_2S_3 at 8 K [7]. The fit at and above the boson peak can be improved considerably if the Gaussian form assumed by MB for the correlation functions is replaced by an exponential or Lorentzian function, as shown by Malinovsky and Sokolov [1].

In Fig. 3, we show our experimental *VV* spectrum of the 15% LiCl sample at 100 K, with a fit to Eq. (10a) in the frequency range 10–55 cm^{-1}. In the fitting procedure, we used values of v_l and v_t obtained from our recent Brillouin-scattering experiments [38]. The structural correlation length found from the fit was $\sigma\sim3$ Å, which is comparable to the $O\text{-}Cl^-$ distance of ~3.3 Å, and the $O\text{-}Li^+$ distance of ~2 Å [43].

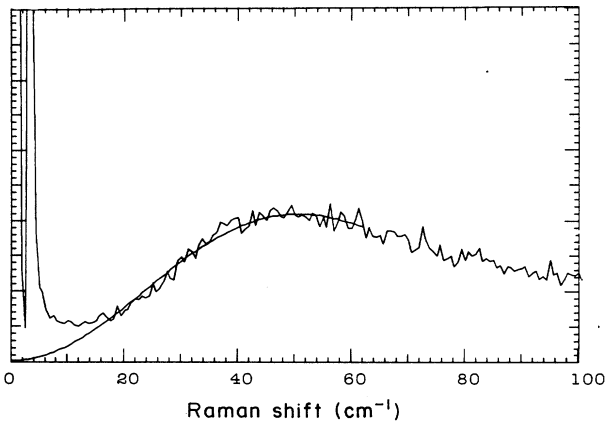

FIG. 3. Stokes Raman spectrum of 15 mol % LiCl solution in the glass phase at $T=100$ K, with a fit to the Martin-Brenig prediction of Eq. (10a).

2. *Depolarization ratio*

The Martin-Brenig result of Eqs. (10) predicts a depolarization ratio $\rho(\omega)=I^{VH}(\omega)/I^{VV}(\omega)$ of [7]

$$\rho(\omega)=\left[\frac{4}{3}+\frac{30}{2+3g_t/g_l}\left[\frac{(\delta p_l)^2+\lambda p_l^2}{(\delta p_t)^2+\lambda p_t^2}\right]\right]^{-1}. \quad (11)$$

Martin and Brenig also suggested that $(\delta p_l)^2/p_l^2 \cong (\delta p_t)^2/p_t^2$, which reduces Eq. (11) to

$$\rho(\omega)=\left[\frac{4}{3}+\frac{30}{2+3g_t/g_l}\left[\frac{p_l^2}{p_t^2}\right]\right]^{-1}. \quad (12)$$

Note that the depolarized scattering is entirely due to the transverse-acoustic modes. If $p_t=0$, then from Eq. (10b), $I_s^{VH}(K,\omega)=0$, and the depolarization ratio, from Eq. (11) or (12), is $\rho(\omega)=I^{VH}/I^{VV}=0$.

To obtain numerical predictions for the low-frequency value of $\rho(\omega)$ from Eq. (12) requires values for (p_l/p_t) and (v_l/v_t) which can both be obtained from Brillouin-scattering data. From Eqs. (5), the ratio of the integrated intensities for LA (VV) and TA (VH) Brillouin scattering is

$$\frac{I_{VV}}{I_{VH}}=8\left[\frac{v_t}{v_l}\right]^2\frac{p_{12}^2}{(p_{11}-p_{12})^2},$$

from which

$$\frac{p_l}{p_t}=\frac{1}{\sqrt{8}}\left[\frac{v_l}{v_t}\right]\left[\frac{I_{VV}}{I_{VH}}\right]^{1/2}+\frac{1}{3},$$

with the values $v_l/v_t=2.06$ and $p_l/p_t=4.70$ found from our Brillouin-scattering experiments [38]. Equation (12) predicts that for ω well below the peak at 55 cm^{-1}, $\rho(\omega\rightarrow 0)_{\rm MB}=0.14$, approximately six times smaller than our experimental result of 0.8 (see Table I). Furthermore, since in Eq. (12) g_t and g_l are functions of frequency, the predicted depolarization ratio would be frequency dependent, which also disagrees with our results.

In Fig. 2(c) we have superimposed a dashed line showing the prediction of Eq. (12) increased by a factor of 5.7 to match the experimental depolarization ratio at low frequencies. A similar disagreement was noted by Nemanich [7] for several chalcogenide glasses. The observed depolarization ratios for these materials was ~ 0.5 and was essentially independent of frequency, while the Martin-Brenig prediction at $\omega\rightarrow 0$ was ~ 0.1 and decreases with increasing frequency.

We have performed Brillouin-scattering measurements on several other materials besides the LiCl solutions and used the results to further test the MB prediction of Eq. (12). In Table I we show our experimental depolarization ratios for 15% LiCl solution, quartz, salol, and 40 mol % $Ca(NO_3)_2$–60 mol % KNO_3 (CKN). LiCl, salol, and CKN, all of which are fragile materials, gave experimental depolarization ratios of $\sim\frac{3}{4}$, while the MB predictions at $\omega\rightarrow 0$ are 0.14, 0.27, and 0.17, consistently too small. Only quartz, which is a network glass, gave reasonable agreement at $\omega\rightarrow 0$, as previously reported by Winterling [5]. However, Eq. (12) predicts a fairly strong frequency dependence for all these materials including quartz, which we did *not* observe.

TABLE I. Depolarization ratio $\rho(\omega)$ from Raman scattering experiments and the MB prediction at $\omega\rightarrow 0$ from Brillouin scattering measurements of v_l/v_t and I_{VV}/I_{VH}. The correlation length σ was found from fits to Eq. (10). LiCl=15% aqueous LiCl solution. CKN=$0.4Ca(NO_3)_2-0.6KNO_3$ ($T_g=333$ K). CKN does not display a clearly defined Boson peak.

	LiCl	Quartz	Salol	CKN
$\rho(\omega)_{\rm expt}(3\lesssim\omega\leq 100$ cm$^{-1})$	0.80	0.22	0.75	0.75
T (K) (Raman)	150	300	193	300
v_l/v_t (Brillouin)	2.06	1.58	2.33	2.14
I_{VV}/I_{VH} (Brillouin)	35.9	9.58	20.7	32.4
T (K) (Brillouin)	78	300	193	300
p_l/p_t	4.70	2.06	4.08	4.64
$\rho(\omega\rightarrow 0)_{\rm MB}$	0.14	0.19	0.27	0.17
σ (Å)	2.7	3.9	6.8	*

3. *Intensity*

Theodorakopoulos and Jackle [16] estimated the scattering intensity predicted by the Martin-Brenig model due to electrical disorder alone, neglecting mechanical disorder ($\lambda=0$). They showed that for SiO_2 glass the predicted intensity is ~ 3000 times smaller than the experimental intensity at ~ 20 cm^{-1} measured by Winterling [5]. They assumed that the disorder is determined by the spatially fluctuating density $\delta\rho(x)$, which freezes at the glass transition temperature T_g, so that for temperatures below T_g, $(\delta\rho)^2/\rho^2 = k_B T_g \kappa_T$, where κ_T is the isothermal compressibility at T_g. They also asserted that $(\delta p)^2/p^2 \simeq (\delta\rho)^2/\rho^2$.

We can similarly estimate the disorder-induced-scattering intensity for LiCl solutions from Eq. (10a) with $(\delta p)^2/p^2 = k_B T_g \kappa_T$ in which $T_g = 140$ K and $\kappa_T(T_g) = 1.0\times 10^{-12}$ dyn^{-1} cm^2 [38]. From Eqs. (5a) and (10a) we estimate that at 140 K the ratio of the integrated disorder-induced VV Raman-scattering intensity (integrated from 0 cm^{-1} to the peak at $v_t/2\pi c\sigma$) to the integrated polarized Brillouin peak is $\sim 10^{-4}$, which is at least 1000 times smaller than the experimental value.

Theodorakopoulous and Jackle [16] suggested two possible explanations for the disagreement with the intensity prediction of the Martin-Brenig model: (i) mechanical disorder may play a much larger role than electrical disorder, and (ii) frozen-in anisotropy fluctuations may be more important than frozen-in density fluctuations.

MB showed that $\lambda \cong \langle (\delta E)^2/E^2 \rangle$, where E is the Young's modulus. Since $E = \rho v_l^2 = \rho\omega_l^2/q^2$, the fluctuation in E due to the frozen density fluctuations $\delta\rho$ would be $\delta E = [\rho\delta(\omega_l^2) + \omega_l^2\delta\rho]/q^2$ so that

$$\lambda = \left[\left\langle \left[\frac{\delta(\omega_l^2)}{\omega_l^2} \right]^2 \right\rangle + \left\langle \frac{(\delta\rho)^2}{\rho^2} \right\rangle \right] = \frac{\langle (\delta\rho)^2 \rangle}{\rho^2} (2\gamma+1)^2 ,$$

where $\gamma = \partial \ln(\omega_l)/\partial \ln(\rho)$ is the Gruneisen constant for longitudinal-acoustic modes, which is of order unity [44]. Therefore, the contribution of mechanical disorder to the scattered intensity cannot be much more than approximately ten times larger than the contribution of electrical disorder, leaving a residual disagreement of greater than 100. As for anisotropy fluctuations, LiCl solutions consist of molecules that are essentially optically isotropic. Experimentally, scattering from LiCl solutions due to fluctuations in optical anisotropy has been found to be approximately 100 times weaker than scattering due to density fluctuations [45]. Therefore, we conclude that the predictions of the MB model for both the depolarization ratio and the scattered intensity are in serious disagreement with our experimental results.

Finally, we note that the correlation lengths shown in Table I, found from fitting the MB equations to the shape of the Raman spectra, typically turn out to be on the order of interatomic distances. Similar results have been found previously in other experiments [1,7,9]. However, as pointed out by Pick [46], the MB theory is a continuum approximation, and it is inconsistent to extend it to wavelengths comparable to interatomic separations where both the lattice dynamics and light scattering require a microscopic description.

Such a microscopic description [47] may provide an improved version of the MB theory. However, in the long-wavelength limit, where the MB continuum approach should be valid, the disagreement with experiment for the depolarization ratio must have a different origin.

IV. GENERALIZED HYDRODYNAMICS MODEL

Because the central predictions of the disordered-crystal model discussed in Sec. III are in serious disagreement with our experimental results, and since there is no straightforward way to extend this model to the liquid phase above T_g, we consider an alternative theory of the low-frequency Raman spectrum based on hydrodynamics rather than lattice dynamics. We note that while a general theory of the lattice dynamics of glasses has not yet been developed, the dynamics of liquids have been found to be quite well described by molecular hydrodynamics [48], which reduces to classical hydrodynamics at small **q** and to kinetic theory at large **q**.

Recently, using the mode-coupling approximation to include nonlinear interactions, molecular hydrodynamics has been extended to describe the liquid-glass transition [49–51]. This mode-coupling theory of the glass transition predicts a purely kinetic transition with no drastic structural change, and also describes the evolution of the dynamics through the glass transition.

The central concept in the mode-coupling theory of the glass transition is that nonlinearity causes coupling between density fluctuation modes, especially those whose wave vectors are within the main peak of the structure factor $S(q)$ with $q \approx q_0$. With decreasing temperature (or increasing density) this nonlinear interaction leads to a slowing down of these density fluctuations, which eventually freeze at the glass transition temperature.

In a simple fluid, the fluctuations $\delta\epsilon$ in the (isotropic) dielectric constant are related to the number density fluctuations δn by

$$\delta\epsilon = \left[\frac{\partial\epsilon}{\partial n} \right] \delta n + \frac{1}{2} \left[\frac{\partial^2\epsilon}{\partial n^2} \right] (\delta n)^2 + \ldots . \tag{13}$$

The first term in Eq. (13), when substituted into Eq. (1), yields

$$R^{(1)}(K,\omega) = \left[\frac{\omega_s}{c} \right]^4 \frac{1}{16\pi^2} \left[\frac{\partial\epsilon}{\partial n} \right]^2 nS(K,\omega)(\hat{\mathbf{E}}_s \cdot \hat{\mathbf{E}}_0) , \tag{14}$$

where $\hat{\mathbf{E}}_0$ and $\hat{\mathbf{E}}_s$ are unit vectors in the directions of the incident and scattered electric fields (for 90° scattering, $\hat{\mathbf{E}}_0 \cdot \hat{\mathbf{E}}_s = 1$ for VV, 0 for VH) and $S(K,\omega) = (1/n)\langle (\delta n)^2 \rangle_{K\omega}$ is the dynamic structure factor, the space-time Fourier transform of the density-density correlation function.

In Stephen's analysis [17,18], the atomic polarizability α was used instead of $(\partial\epsilon/\partial n)$. These two quantities are related by the Lorentz-Lorenz formula $(\epsilon-1)/(\epsilon+2)$

$=(4\pi/3)\alpha n$, from which $(\partial\epsilon/\partial n)=(4\pi/9)\alpha(\epsilon+2)^2$.

Stephen's result for the first-order scattering is

$$R^{(1)}(K,\omega)=\left[\frac{\omega_s}{c}\right]^4\alpha^2(\hat{\mathbf{E}}_s\cdot\hat{\mathbf{E}}_0)nS(K,\omega)\ . \tag{15}$$

[Note that with Stephen's definition of $S(K,\omega)$ the factor of n in Eq. (15) would be missing.]

Stephen analyzed the scattering due to a second-order DID process in which the electric field of the incident light polarizes the atoms taking part in a first density fluctuation with wave vector $\mathbf{q}$. This polarization gives rise to an electric field at a second density fluctuation with wave vector $\mathbf{K}-\mathbf{q}$, which in turn produces the scattered field. Stephen's result for this two-step second-order Raman spectrum is

$$R^{(2)}(K,\omega)=\left[\frac{\omega_s}{c}\right]^4\alpha^4\tfrac{6}{5}[1+\tfrac{1}{3}(\hat{\mathbf{E}}_s\cdot\hat{\mathbf{E}}_0)^2]\times(1/2\pi)^4\times\int\int d^3q\,d\omega' g^2(q)nS(q,\omega')\times nS(K-q,\omega-\omega')\ , \tag{16}$$

where the factor $g(q)=4\pi[\sin(qa)/(qa)^3-\cos(qa)/(qa)^2]$ results from excluding from the integration a sphere of radius a approximately equal to one-half the interparticle spacing, to avoid inclusion of self-polarization. In arriving at Eq. (16), a four-point density fluctuation correlation function was factored into a sum of products of two-point correlation functions.

One strong piece of evidence for the relevance of this approach to the low-frequency Raman spectrum of aqueous LiCl solutions (and probably to other fragile glass formers as well) is the molecular-dynamics analysis of Madden and Impey [21]. They calculated the Raman spectrum of water due to the dipole–induced-dipole mechanism and found broad bands centered near 60 and 180 cm^{-1} as observed in the experiments.

We shall explore the predictions of Eq. (16), assuming that it applies to both the liquid and the glass phases, in the spirit of the mode-coupling theory of the glass transition.

A. Depolarization ratio

Since for polarized (VV) scattering $\hat{\mathbf{E}}_0\cdot\hat{\mathbf{E}}_s=1$, while for 90° depolarized (VH) scattering $\hat{\mathbf{E}}_0\cdot\hat{\mathbf{E}}_s=0$, Eq. (16) predicts that the depolarization ratio for 90° scattering is a frequency- and material-independent constant [18]

$$[\rho(\omega)]_{90^\circ}=0.75\ , \tag{17}$$

in excellent agreement with our LiCl data as well as our salol and CKN data. We also note that Eq. (17) is in much better agreement with the experimental results for chalcogenide glasses [7] than the disordered-crystal-model prediction of Eq. (12), although the hydrodynamic model is not expected to apply directly to network glasses.

Note that in contrast to the disorder-induced-scattering model discussed in Sec. III, the second-order DID Raman-scattering process has a frequency-independent depolarization ratio of 0.75 due to longitudinal-acoustic modes alone, without requiring any transverse modes.

B. Scattered intensity

The integrated spectrum of the second-order polarized Raman scattering of Eq. (16) can be compared to the integrated Brillouin spectrum of Eq. (14) without specifying the frequency dependence of $S(q,\omega)$. Integrating these expressions over frequency, we find

$$R^{(1)}(K)=2\pi\left[\frac{\omega_0}{c}\right]^4\alpha^2(\hat{\mathbf{E}}_0\cdot\hat{\mathbf{E}}_s)^2nS(K)\ , \tag{18}$$

$$R^{(2)}(K)=\frac{1}{(2\pi)^2}\left[\frac{\omega_0}{c}\right]^4\alpha^4\tfrac{6}{5}[1+\tfrac{1}{3}(\hat{\mathbf{E}}_0\cdot\hat{\mathbf{E}}_s)]\times\int d^3q\,g^2(q)n^2S^2(q)\ , \tag{19}$$

where we have approximated $\mathbf{K}-\mathbf{q}$ by $-\mathbf{q}$ and ω_s by ω_0, and where $S(q)=(1/2\pi)\int d\omega S(q,\omega)$. The structure factor $S(q)$ in liquids usually has a sharp peak at a value of $q=q_0$ corresponding approximately to the average interatomic distance, which dominates the integral in Eq. (19). We can therefore approximate Eq. (19) by

$$R^{(2)}(K)=\frac{1}{(2\pi)^2}\left[\frac{\omega_0}{c}\right]^4\alpha^4\tfrac{6}{5}[1+\tfrac{1}{3}(\hat{\mathbf{E}}_0\cdot\hat{\mathbf{E}}_s)]\times 4\pi q_0^2 g^2(q_0)n^2S^2(q_0)\Delta q_0\ , \tag{20}$$

where q_0 is the wave vector of the peak and Δq_0 is its width.

For VV scattering, the intensity ratio predicted by Eqs. (18) and (20) is

$$\left[\frac{I^{(2)}(K)}{I^{(1)}(K)}\right]_{VV}=\frac{\alpha^2}{(2\pi)^2}\frac{16}{5}q_0^2\Delta q g^2(q_0)\frac{nS^2(q_0)}{S(K)}\ . \tag{21}$$

To evaluate Eq. (21), we used the Percus-Yevick approximation for a hard-sphere gas [52] to find q_0, $S(q_0)$, Δq_0, and $S(K\sim 0)$. For hard spheres of diameter σ at a density corresponding to $T\cong 150$ K, we find [38] $q_0\sim 7/\sigma$, $\Delta q_0\cong 1/\sigma$, $S(q_0)\cong 3.5$, and $S(K\sim 0)\cong 0.014$. With these values, Eq. (21) reduces to $12.5g^2(q_0)$.

The value of $g(q_0)$ is very sensitive to the choice of the radius a of the excluded volume. If we use the packing fraction at the glass transition, $\Psi_c=0.516$ to estimate the mean interparticle separation at 1.128σ, then $q_0a=3.95$, $g(q_0)=0.167$, and

$$\left[\frac{I^{(2)}(K)}{I^{(1)}(K)}\right]_{VV}\simeq 2.1\ ,$$

which is ~ 20 times larger than the experimental value of 0.1. However, by increasing q_0a to 4.3, the result would be 0.2, quite close to our experimental result. In view of the sensitive dependence of $I^{(2)}$ on the value of the unknown parameter a, this aspect of the analysis provides only qualified agreement and cannot be accurately tested.

C. The spectrum

The spectrum $R^{(2)}(K,\omega)$ given by Eq. (16) is determined by the dynamic structure factor $S(q,\omega)$, the Fourier transform of the intermediate scattering function $F(q,t)$. In generalized (or molecular) hydrodynamics, $S(q,\omega)$ is the real part of $S(q)\tilde{R}(q,\omega)$, where

$$\tilde{R}(q,\omega)=i\Big/\left[\omega-\frac{\Omega_0^2(q)}{\omega+i\tilde{M}(q,\omega)}\right], \tag{22}$$

where $\Omega_0^2(q)=(qv_0)^2/S(q)$, $v_0=k_BT/m$ is a molecular velocity, and $\tilde{M}(q,\omega)$ is a generalized friction function. [In Eq. (22), the effects of temperature fluctuations, which produce additional structure at very low frequencies, have been neglected.] Writing $F(q,t)=\phi(q,t)S(q)$, Eq. (22) is equivalent to the equation of motion for the normalized correlation function $\phi(q,t)$:

$$\ddot{\phi}(q,t)+\gamma\dot{\phi}(q,t)+\Omega_0^2\phi(q,t)+\int_0^t M(q,\tau)\dot{\phi}(q,t-\tau)d\tau=0\ . \tag{23}$$

In Eq. (23), the nonrelaxing part of $M(q,\tau)$ has been separated as γ, and $\dot{\phi}$ and $\ddot{\phi}$ are the first and second time derivatives of $\phi(q,t)$. The longitudinal memory function $M(q,t)$ in Eq. (23) is usually represented phenomenologically as a single relaxation function (Maxwell viscoelasticity) or as a two relaxation time function [36,53].

In the mode-coupling theory, the excess damping introduced by the integral in Eq. (23) is associated with nonlinear interactions between modes, and the memory function is [51]

$$M(q,\tau)=\sum_{q_1,q_2\cdots}[V^{(1)}(q,q_1)\phi(q_1,\tau)+V^{(2)}(q,q_1,q_2)\phi(q_1,\tau)\phi(q_2,\tau)+\cdots]\ . \tag{24}$$

In the simplest version of the mode-coupling theory [49,50], only the third-order nonlinear interaction term $V^{(2)}$ is retained, and only modes with a single q are included, so that Eq. (23), for $q=q_0$, becomes

$$\ddot{\phi}(q_0,t)+\gamma\dot{\phi}(q_0,t)+\Omega_0^2\phi(q_0,t)+\int_0^t V^{(2)}(q_0)\phi^2(q_0,\tau)\dot{\phi}(q_0,t-\tau)d\tau=0\ . \tag{25}$$

Equation (25), which was first proposed by Leutheusser [50], is designated as the F_2 model by Gotze [51]. It is a simplified version of the mode-coupling theory which lacks some important aspects of more sophisticated models [51].

In order to explore the relevance of Eq. (25) to the temperature evolution of the Raman spectra in the liquid and glass phases, we show, in Fig. 4(a), three of our 30% LiCl Raman spectra, at 270, 220, and 78 K, above, near, and well below the liquid-glass transition at 165 K. In Fig. 4(b), we show $\chi''(\omega)=I(\omega)/[n(\omega)+1]$ [where $n(\omega)$ is the Bose factor] for these same three spectra. Note that while only the 78-K spectrum exhibits a well-defined peak near 55 cm^{-1}, this peak is clearly present in all three $\chi''(\omega)$ plots. To further motivate the association of

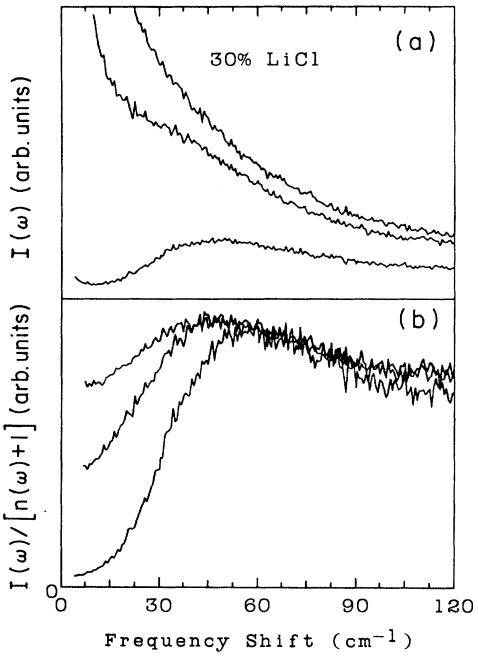

FIG. 4. (a) Raman spectra of 30% LiCl solution ($T_g=165$ K) at (top to bottom) $T=270$, 220, and 78 K. (b) $\chi''(\omega)=I(\omega)/[n(\omega)+1]$ for the three spectra of (a).

these Raman spectra with $S(q_0,\omega)$, we note that a recent inelastic neutron-scattering study of the liquid-glass transition in the protein myoglobin [54] revealed that $S(q,\omega)$ at $q=1.5$ $Å^{-1}$ exhibits an evolution with temperature very similar to our LiCl Raman spectra.

In order to predict theoretical Raman spectra from Eq. (25), we first solved Eq. (25) numerically with $\gamma=\Omega_0=160$ cm^{-1} and $V^{(2)}(q_0)=4\lambda\Omega_0^2$. The glass transition then corresponds to $\lambda_c=1.0$ [50].

In Fig. 5, we show plots of $\phi(q_0,t)$ found from these numerical solutions with λ between 0.1 and 2.0. This figure, which closely resembles that of Leutheusser [50], shows that as λ increases towards $\lambda_c=1$, the decay of $\phi(q_0,t)$ becomes slower, while for $\lambda>\lambda_c$ in the glass phase, $\phi(q_0,t)$ decays towards a nonzero infinite-time value $\phi(q_0,\infty)=f$, the nonergodic fraction.

Equation (16) for $R^{(2)}(K,\omega)$, with the approximation that only modes with $q=q_0$ need be retained in the integral, becomes

$$R^{(2)}(K,\omega)=\left[\frac{\omega_s}{c}\right]^4\frac{\alpha^4}{(2\pi)^4}\frac{8}{5}g^2(q_0)4\pi q_0^2\Delta q_0\times\int d\omega' nS(q_0,\omega')S(-q_0,\omega-\omega')\ . \tag{26}$$

The convolution $S(q_0,\omega)\otimes S(q_0,\omega)$ in Eq. (26) was obtained from the computed $\phi(q_0,t)$ data illustrated in Fig. 5 by squaring $\phi(q_0,t)$ and then Fourier transforming the result. Before performing the transformation, the constant background $f^2=\phi^2(q_0,\infty)$ for $\lambda>1$, which produces an elastic peak $A\delta(\omega)$, was subtracted. The re-

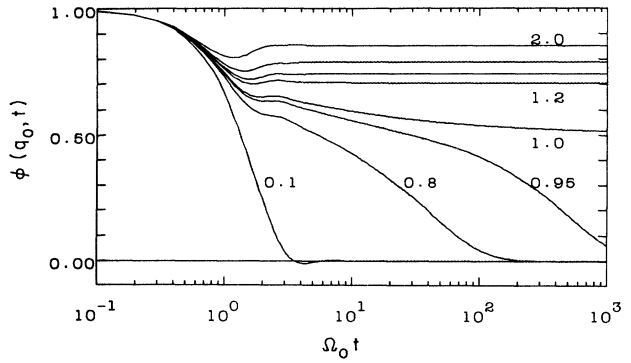

FIG. 5. $\phi(q_0,t)$ vs $\Omega_0 t$ from Eq. (25) with $\gamma=\Omega_0=160$ cm^{-1} and $V^{(2)}(q_0)=4\lambda\Omega_0^2$. λ ranges from 0.1 to 2.0 (the transition is at $\lambda_c=1.0$).

sults, which are proportional to Eq. (26), are shown in Fig. 6 for λ between 0.8 and 2.0.

These theoretical spectra, though only qualitative, exhibit the main features of the experimental spectra of Fig. 1 in the frequency range of 3–100 cm^{-1}. At high temperature there is a broad central peak with a weak shoulder. With decreasing temperature (i.e., increasing λ) the central peak narrows, while the shoulder develops into a broad peak near 50 cm^{-1} with a long tail on the high-frequency side, becoming underdamped in the glass phase.

We also note that the theoretical spectra predicted by Eqs. (25) and (26) do not go to zero as $\omega\rightarrow 0$, in agreement with the excess scattering phenomenon first noted

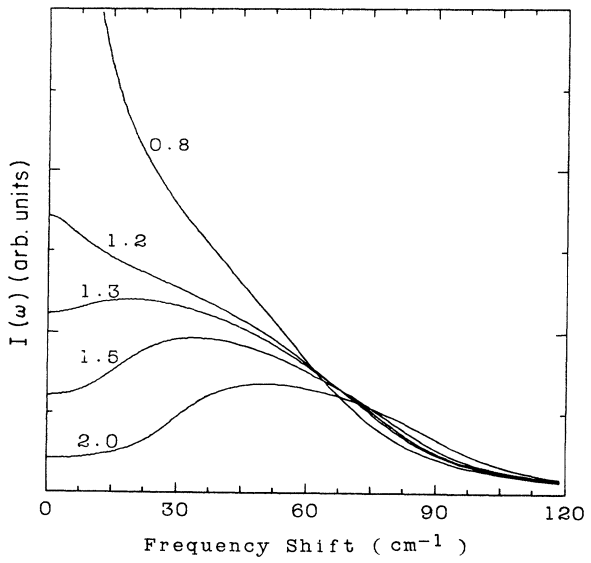

FIG. 6. Theoretical Raman spectra predicted by Eq. (26). The convolution $S(q_0,\omega)\otimes S(q_0,\omega)$ was found by Fourier transformation of $\phi^2(q_0,t)$ found from Eq. (25) with values of λ between 0.8 and 2.0.

by Winterling [5], and that this excess scattering also decreases with decreasing temperature in the glass phase, as shown in Fig. 6.

V. SUMMARY AND CONCLUSIONS

The low-frequency Raman spectra, depolarization ratios, and ratios of the integrated Raman intensities to integrated Brillouin intensities were investigated in 15 and 30 mol % aqueous LiCl solutions in both the liquid and glass phases. The similarity between these spectra and the Raman spectrum of pure water suggests a common origin for the principal features of both. Furthermore, since the low-temperature spectra we obtained are very similar to the usual Raman spectra of glasses, we conclude that the bands near 55 cm^{-1} in water and in glasses also have a common origin. Similarly, the fact that the central peak and the 55-cm^{-1} band observed in the glass phase have the same depolarization ratio also suggests that these features have a common origin.

We compared our results with the disorder-induced-scattering model as formulated by Martin and Brenig, and found that a reasonable fit to the spectral shape in the glass can be achieved if the central peak is excluded. However, the observed Raman intensity at $\sim$20 cm^{-1} is at least 100 times higher than the theory predicts. Furthermore, our experimentally observed depolarization ratio of $\sim$0.8 is much larger than the predicted value of $\sim$0.14.

In our comparison with a hydrodynamic model based on Stephen's theory, we found excellent agreement for the depolarization ratio, and qualified agreement for the Raman intensity, which depends critically on the excluded volume chosen. By combining Stephen's model with generalized hydrodynamics and mode-coupling concepts, we were also able to demonstrate qualitative agreement with the spectral shape in both the liquid and glass phases, including the continuous transformation of the broad central peak found in the liquid into a broad band near 55 cm^{-1} in the glass. The additional low-frequency structure is presumably associated with the beta-relaxation process, which is present in both the liquid and glass phases. In the glass phase, beta relaxation may be equivalent to the relaxing defect mechanism.

The most definitive difference between the two theoretical models described is their very different predictions for the depolarization ratio. In Stephen's hydrodynamic DID theory, the scattering is a second-order process resulting in a universal depolarization ratio of 0.75 (for 90° scattering), independent of frequency and of material properties. The Martin-Brenig theory, in contrast, is a first-order scattering theory, and the depolarization ratio depends critically on the relative strengths of transverse and longitudinal Brillouin scattering. Since we have measured these strengths independently for our samples, we could show that for aqueous LiCl the predicted depolarization ratio is $\sim$0.14, far smaller than our measured value of $\sim$0.8. We believe that this prediction provides strong evidence in favor of the hydrodynamic theory.

Finally, we note that the dynamics of glasses are very

complicated, with both spatially extended and localized modes present, and that a complete theory of light scattering in glasses is not yet available. What we have shown is that the hydrodynamic theory is capable of explaining the low-frequency spectrum in both the liquid and glass phases, at least qualitatively, and therefore of explaining the continuous evolution of the spectrum with decreasing temperature.

ACKNOWLEDGMENTS

We wish to acknowledge helpful discussions with Robert Pick, Paul Fleury, Michael Stephen, Christianne Alba, and Catherine Dreyfus. This research was supported by NSF Grant No. DMR-8614168, and in part by the Science Division and Physics Department of the City College of the City University of New York.

[1] V. K. Malinovsky and A. P. Sokolov, Solid State Commun. **57**, 757 (1986).
[2] P. W. Anderson, B. I. Halperin, and C. M. Varma, Philos. Mag. **25**, 1 (1972).
[3] W. A. Phillips, J. Low. Temp. Phys. **7**, 351 (1972).
[4] N. Theodorakoupoulos and J. Jackle, Phys. Rev. B **6**, 2637 (1976).
[5] G. Winterling, Phys. Rev. B **12**, 2432 (1975).
[6] A. Fontana, L. M. Gratton, and C. Tosello, in *Dynamics of Disordered Materials,* edited by D. Richter, A. J. Dianoux, W. Petry, and J. Teixeira (Springer-Verlag, Berlin, 1989), p. 221.
[7] R. J. Nemanich, Phys. Rev. B **16**, 1655 (1977).
[8] H. Kawamura, K. Fukumasu, and Y. Hamada, Solid State Commun. **43**, 229 (1982).
[9] F. Viras and T. A. King, J. Non-Cryst. Solids **119**, 65 (1990).
[10] R. Shuker and R. W. Gammon, J. Chem. Phys. **55**, 4784 (1971).
[11] F. Aliotta, G. Maisano, P. Migliardo, C. Vasi, F. Wanderlingh, G. P. Smith, and T. Triolo, J. Chem. Phys. **75**, 613 (1981).
[12] V. Mazzacurati, M. Nardone, and G. Signorelli, J. Chem. Phys. **66**, 5380 (1977).
[13] C. V. Raman and K. S. Krishnan, Nature **122**, 278 (1928).
[14] H. B. Levine and G. Birnbaum, Phys. Rev. Lett. **20**, 439 (1968).
[15] J. P. McTague, P. A. Fleury, and D. B. DuPre, Phys. Rev. **188**, 303 (1969).
[16] M. Thibeau, B. Oskengorn and B. Vodar, J. Phys. (Paris) **29**, 287 (1968).
[17] M. J. Stephen, Phys. Rev. **187**, 279 (1969).
[18] M. J. Stephen, in *The Physics of Liquid and Solid Helium,* edited by K. H. Bennemann and J. B. Ketterson (Wiley, New York, 1976), p. 307.
[19] T. J. Greytak and J. Yan, Phys. Rev. Lett. **22**, 987 (1969).
[20] R. W. Impey, P. A. Madden, and I. R. McDonald, Mol. Phys. **46**, 513 (1982).
[21] P. A. Madden and R. W. Impey, Chem. Phys. Lett. **123**, 502 (1986).
[22] P. A. Madden, Mol. Phys. **36**, 365 (1978).
[23] P. A. Madden and J. A. Board, J. Chem. Soc. Faraday Trans. (2) **83**, 891 (1987).
[24] P. A. Madden and K. O'Sullivan, J. Phys. Condens. Matter **2**, SA257 (1990).
[25] J. Giergiel, K. R. Subbaswamy, and P. C. Eklund, Phys. Rev. B **29**, 3490 (1984).
[26] C. A. Angell and E. J. Sare, J. Chem. Phys. **49**, 4713 (1968); C. A. Angell, E. J. Sare, J. Donnella, and D. R. MacFarlane, J. Phys. Chem. **85**, 1481 (1981).
[27] A. DeSantis, R. Frattini, M. Sampoli, V. Mazzacurati, M. Nardone, M. A. Ricci, and G. Ruocco, Mol. Phys. **61**, 1199 (1987).
[28] R. Shuker and R. W. Gammon, Phys. Rev. Lett. **25**, 222 (1970).
[29] R. C. Zeller and R. O. Pohl, Phys. Rev. B **4**, 2029 (1971).
[30] F. Aliotta, C. Vasi, G. Maisano, D. Majolino, F. Mallamace, and P. Migliardo, J. Chem. Phys. **84**, 4731 (1986).
[31] B. Benassi, V. Mazzacurati, M. Nardone, M. A. Ricci, G. Ruocco, A. DeSantis, R. Frattini, and M. Sampoli, Mol. Phys. **62**, 1467 (1987).
[32] S. Krishnamury, R. Bansil, and J. Wiafe-Akenten, J. Chem. Phys. **79**, 5863 (1983).
[33] J. L. Rousset, E. Duval, and A. Boukenter, J. Chem. Phys. **92**, 2150 (1990).
[34] G. E. Walrafen, J. Chem. Phys. **40**, 3249 (1964).
[35] C. J. Montrose, J. A. Bucaro, J. Marshall-Coakley, and T. A. Litovitz, J. Chem. Phys. **60**, 5025 (1974).
[36] G. E. Walrafen, M. S. Hokmabadi, W.H. Yang, Y. C. Chu, and B. Monsmith, J. Phys. Chem. **93**, 2909 (1989).
[37] E. Whalley and J. E. Bertie, J. Chem. Phys. **46**, 1264 (1967).
[38] N. J. Tao, G. Li, and H. Z. Cummins, Phys. Rev. B **43**, 5815 (1991).
[39] W. Hayes and R. Loudon, *Scattering of Light by Crystals* (Wiley, New York, 1978).
[40] H. Z. Cummins and P. E. Schoen, in *Laser Handbook,* edited by F. T. Arecchi and E. O. Schultz-Dubois (North-Holland, Amsterdam, 1971), p. 1029.
[41] R. J. Nemanich, J. Non-Cryst. Solids **59-60**, 851 (1983).
[42] A. J. Martin and W. Brenig, Phys. Status Solidi B **64**, 163 (1974).
[43] J. E. Enderby and G. W. Neilson, Rep. Prog. Phys. **44**, 38 (1981).
[44] N. W. Ashcroft and N. D. Mermin, *Solid State Physics* (Saunders, Philadelphia, 1976), p. 494.
[45] N. J. Tao and S. M. Lindsay, J. Phys. Condens. Matter **1**, 8709 (1989).
[46] R. M. Pick (private communication).
[47] V. Mazzacurati, M. Nardone, G. Ruocco, and G. Signorelli, Philos. Mag. B **59**, 3 (1989).
[48] J. P. Boon and S. Yip, *Molecular Hydrodynamics* (McGraw-Hill, New York, 1976).
[49] U. Bengtzelius, W. Gotze, and A. Sjolander, J. Phys. C **17**, 5915 (1984).
[50] E. Leutheusser, Phys. Rev. A **29**, 2765 (1984).
[51] For a recent comprehensive review of the mode-coupling theory of the glass transition, see W. Gotze, in *Liquids, Freezing, and the Glass Transition,* edited by J. P. Hansen, D. Levesque and J. Zinn-Justin (North-Holland, Amsterdam, 1990).
[52] N. W. Ashcroft and J. Lekner, Phys. Rev. **145**, 83 (1966).
[53] D. Levesque, L. Verlet, and J. Kurkijarvi, Phys. Rev. A **7**, 1690 (1973).
[54] W. Doster, S. Cusak, and W. Petry, Phys. Rev. Lett. **65**, 1080 (1990).